JOURNAL OF SOLID STATE CHEMISTRY 118, 66–73 (1995)

A TEM Study of Rhombohedral β Type Solid Solutions in the Bi_2O_3–SrO and Bi_2O_3–CaO Systems

R. L. Withers and H. Rossell†

Research School of Chemistry, Australian National University, Canberra, A.C.T. 0200 Australia

Received September 6, 1994; in revised form January 17, 1995; accepted January 17, 1995

Specimens within the $(1-x)BiO_{1.5} \cdot xMO$ (M = Sr, Ca) rhombohedral β type solid solution fields have been synthesized and studied via TEM and powder XRD. Two distinct, fully three-dimensionally ordered, triclinic superstructure phases have been found for both the M = Sr and M = Ca systems. The first, S1, occurs for low x specimens whereas the second, S2, occurs for somewhat higher x specimens. In the case of the M = Sr system, a further incommensurately modulated (although somewhat disordered) superstructure phase was also found for $x = 0.25$.

1. INTRODUCTION

Sillen and Aurivillius (1, 2) were the first to discover the existence of a number of grossly nonstoichiometric phases formed by the reaction of Bi_2O_3 with certain divalent metal oxides. They showed that such solid solution phases were based upon a fully occupied cation sublattice with the variable anion to cation ratio being taken up by the anion sublattice. Subsequently, Levin and Roth (3) systematically studied the phase region close to Bi_2O_3 for a variety of M–Bi–O ternary systems and confirmed that wide range, nonstoichiometric solid solutions of average cubic (α) and rhombohedral (β) symmetry readily form in such systems. Takahashi *et al.* (4) have shown that soild solutions of both types are extremely good oxide ion conductors, particularly at temperature above ~700°C.

The focus of this paper is on the second (or β) type of wide range, nonstoichiometric solid solution, first discovered (2) in the Bi_2O_3–BaO system. An order of magnitude jump in the oxide ion conductivity at about 700°C (Takahashi *et al.* (4)) suggested the existence of a subtle polymorphic β_2 to β_1 phase transition in both the Bi_2O_3–SrO and Bi_2O_3–CaO systems. This was subsequently confirmed by Conflant *et al.* (5) and Guillermo *et al.* (6) who found a small but definite discontinuity in the rhombohedral c axis at this phase transition. Conflant *et al.* (5) and Guillermo *et al.* (6) have shown that the low-temperature β_2 polymorph of this phase exists over a composition range $Ca_xBi_{1-x}O_{3/2-x/2}$, $0.12 \leq x \leq 0.19$, in the case of the Bi_2O_3–CaO system (5) and $Sr_xBi_{1-x}O_{3/2-x/2}$, $0.10 \leq x \leq 0.27$, in the case of the Bi_2O_3–SrO system (6). Closely related phases have also been shown to occur in the Bi_2O_3–Sm_2O_3 and Bi_2O_3–La_2O_3 systems (3).

The average structure of such phases was first proposed by Aurivillius (2). Subsequently, Conflant *et al.* (7) and Mercurio *et al.* (8) reported structure determinations of $Sr_{0.235}Bi_{0.765}O_{1.383}$ and $Bi_{0.7}La_{0.3}O_{1.5}$, respectively. While these structure refinements essentially confirmed the earlier model (2) as regards the fully occupied cation distribution, significant uncertainty concerning the anion distribution still remains. The X-ray refinement of $Sr_{0.235}Bi_{0.765}O_{1.383}$, for example, only located about $\frac{2}{3}$ of the oxygen atoms that must be present.

Each of these refinements was based upon rhombohedral $R\bar{3}m$ space group symmetry and used lattice parameters $a \sim 4$ Å and $c \sim 28$ Å (in the hexagonal setting). In the case of Bi_2O_3–MO systems with M a divalent cation, additional satellite reflections indicating the presence of further ordering are known to occur for M = Ba (9) and M = Sr, Ca (10, 11). Various models have been put forward to explain the existence of such additional satellite reflections. Tilley (9), for M = Ba, has suggested that they arise as a result of local Bi, Ba ordering within the mixed metal layers perpendicular to **c** (in the hexagonal setting of the rhombohedral average structure) but that these ordered regions have limited spatial extent and can be regarded as microdomains within a disordered parent structure. Conflant *et al.* (10), on the other hand, propose fully ordered layers perpendicular to **c** but with such ordered layers being uncorrelated along **c** for M = Sr, Ca. Baggio *et al.* (11), for M = Sr, suggest that they are due to a two-dimensional modulation in the basal plane, which is commensurate with the reciprocal lattice of the underlying rhombohedral parent structure for low x but which becomes incommensurate for higher values of x. Finally, Blower and Greaves (12), for a specific composition within

† Dedicated to the memory of Henry Rossell—a fine scientist and human being.

0022-4596/95 $12.00

the M = Ca system, propose a large, fully three-dimensionally ordered, monoclinic supercell.

These various models are far from self-consistent and indeed are often mutually contradictory. For example, there is no agreement as to whether these additional modulations are long-range-ordered along either the hexagonal **c** axis or in the basal plane. The purpose of this paper is to present the results of a detailed TEM study of the modulations characteristic of the rhombohedral β_2 solid solution phase in the Bi_2O_3–SrO and Bi_2O_3–CaO systems.

2. EXPERIMENTAL METHODS

2.1. Sample Preparation

The starting materials (Bi_2O_3 (99.999%, Atomergic) and $CaCO_3$ (99.999%, Halewood) or $SrCO_3$ (99.999%, Cerac)) were calcined overnight at 450°C and stored in a dessicator prior to weighing. Specimens were prepared by grinding together mixtures of the appropriate precalcined starting materials, compacting them, and then firing them in gold vessels at 820–830°C for 4 hr. The resultant pellets were then quenched, reground, repelleted, and annealed at 700°C for 2½ days in the case of Ca or 640°C for 2 days in the case of Sr, i.e., below the β_2 to $\beta 1$ polymorphic phase transition temperature (5, 6). These procedures produced pure, homogeneous, strain-free material with little likelihood of twin structures resulting from the known transformation of the high-temperature β_1 form. In the case of the $Ca_xBi_{1-x}O_{3/2-x/2}$ system, specimens were prepared at x = 0.130 and 0.177 while for the $Sr_xBi_{1-x}O_{3/2-x/2}$ system, specimens were prepared at x = 0.143, 0.200, and 0.250.

2.2. Diffraction Studies

The sample was examined by X-ray powder diffraction (XRPD) using a Guinier–Hägg camera with Cu$K\alpha_1$ radiation. Si (5N) was used as an internal standard. Specimens for TEM observation were obtained by crushing and dispersing onto a holey carbon film. TEM observation was carried out in a JEOL 100CX TEM.

3. RESULTS

3.1. Powder X-Ray Diffraction Results

As previously reported for M = Ba (8), the lines in X-ray powder patterns were always broad for each composition examined and regardless of the annealing time used. Nonetheless the lines observed could all be indexed in terms of an average rhombohedral unit cell. No splitting of these rhombohedral lines, however, was ever detected. The refined unit cell parameters in the hexagonal setting for the various compositions synthesized are given in Table 1.

TABLE 1
Refined Unit Cell Parameters from X-Ray Powder Diffraction Data

x	a (Å)	c (Å)
The $Ca_xBi_{1-x}O_{3/2-x/2}$ system		
0.130	3.966(1)	27.823(10)
0.177	3.939(1)	27.855(9)
The $Sr_xBi_{1-x}O_{3/2-x/2}$ system		
0.143	3.976(1)	28.102(9)
0.200	3.967(1)	28.300(10)
0.250	3.968(1)	28.480(9)

3.2. TEM Results

The well-known "mica-like" morphology of this rhombohedral phase means that selected area electron diffraction patterns (SADPs) taken without tilting are always going to be close in orientation to the **c** axis of the rhombohedral average structure. (Note that here and in what follows all indexing will be with respect to the hexagonal setting of the rhombohedral average structure.) Unlike the results of Tilley (9) for the M = Ba system, the specimens were found to be homogeneous and the electron diffraction patterns obtained were completely reproducible from grain to grain. Superlattice twinning of the type reported by Tilley (9) was never observed and satellite reflections were always present in each grain examined.

Electron diffraction patterns reveal two distinct, fully three-dimensionally ordered, triclinic, superstructure phases for both the M = Sr and M = Ca systems, which we label S1 and S2: S1 for the low x specimens (i.e., x = 0.130 for M = Ca and x = 0.143 for M = Sr) and S2 for the somewhat higher x specimens (i.e., x = 0.177 for M = Ca and x = 0.200 for M = Sr). In the case of the M = Sr system, a further incommensurately modulated (although somewhat disordered) superstructure phase (labeled S3) was also found for the highest value of x (i.e., x = 0.250), in partial agreement with the results of Baggio *et al.* (11). Not enough specimens were grown to determine the width in x of each of these superstructure phases. Nonetheless it is clear that the phase diagrams of both systems are in need of considerable alteration.

Figure 1 shows the central portions (the zero-order Laue zone or ZOLZ regions) of SADPs typical of the S1 phase and taken at the (a) [001] and (b) [$\bar{1}$11] zone axis orientations of the rhombohedral parent structure. The strong Bragg reflections of the underlying rhombohedral parent structure obey the characteristic rhombohedral extinction rule $F(hkl) = 0$ unless $-h + k + l = 3n$ and are clearly visible in both SADPs as are the weak additional superlattice reflections. Somewhat similar SADPs have also been reported by Tilley (9) for the M = Ba system, although we believe that Fig. 3a therein has been incor-

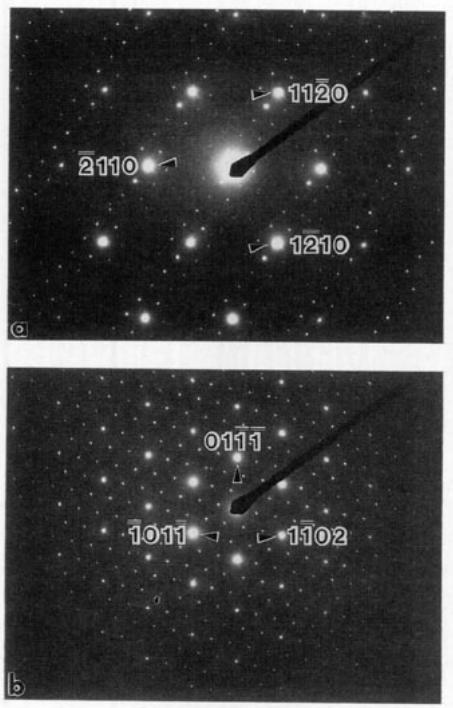

FIG. 1. The zero-order Laue zones (or the ZOLZ regions) of SADPs typical of the S1 phase and taken at the (a) [001] and (b) [−1,1,1] zone axis orientations. The strong reflections corresponding to the rhombohedral parent structure are indexed.

rectly indexed as an [001] rather than a $[\bar{1}11]$ zone axis SADP.

Note that the satellite reflections are not uniformly excited in the ZOLZ region of Fig. 1a whereas they are uniformly excited in the ZOLZ region of Fig. 1b. The banding of the weak superlattice reflections along the $(11\bar{2}0)^*$ direction of reciprocal space in Fig. 1a suggests that a superlattice zone axis orientation can be obtained by tilting about the $(11\bar{2}0)^*$ direction of reciprocal space. Thus Fig. 1b was obtained by tilting Fig. 1a ~13.8° about the $(11\bar{2}0)^*$ direction of reciprocal space. That the satellite reflections are uniformly excited in the ZOLZ region of Fig. 1b is confirmed by the well-defined FOLZ ring visible in the $[\bar{1}11]$ zone axis convergent beam pattern (CBP) corresponding to Fig. 1b and shown in Fig. 2. The FOLZ ring radii in Fig. 2 corresponds to a height along the zone axis direction of $3/|[\bar{1}11]|$ (as would be expected for the rhombohedral substructure reflections but not necessarily for the satellite reflections) and confirms that $3\mathbf{c}^*$ can be chosen to be a reciprocal lattice basis vector of the S1 superstructure. The finding of such substructure zone axis orientations with well-defined ZOLZ regions and HOLZ rings is the key to a correct description of the corresponding reciprocal lattice.

In the language of modulated structures, the reciprocal lattice of this S1 phase can be described in terms of a strong set of rhombohedral parent reflections **G** accompanied by a much weaker set of satellite reflections at $\mathbf{G} \pm \mathbf{q}_j$, where the modulation wave vectors $\mathbf{q}_j$ (see Fig. 1b) characteristic of the superstructure are given by

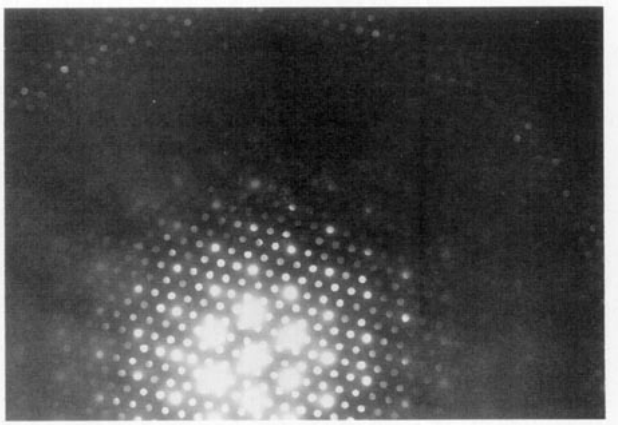

FIG. 2. A [−1,1,1] zone axis orientation CBP corresponding to Fig. 1b. Note the well-defined ZOLZ region and FOLZ ring. The FOLZ ring radii corresponds to a height along the zone axis direction of $3/|[-1,1,1]|$.

$$\mathbf{q}_1 = \tfrac{1}{7}[(01\bar{1}\bar{1})^* - 2(\bar{1}01\bar{1})^*] = \tfrac{1}{7}(2\mathbf{a}^* + \mathbf{b}^* + \mathbf{c}^*)$$

$$\mathbf{q}_2 = \tfrac{1}{7}[(\bar{1}01\bar{1})^* - 2(1\bar{1}02)^*] = \tfrac{1}{7}(-3\mathbf{a}^* + 2\mathbf{b}^* - 5\mathbf{c}^*)$$

and

$$\mathbf{q}_3 = \tfrac{1}{7}[(1\bar{1}02)^* - 2(01\bar{1}\bar{1})^*] = \tfrac{1}{7}(\mathbf{a}^* - 3\mathbf{b}^* + 4\mathbf{c}^*)$$

in terms of the hexagonal basis vectors of the parent rhombohedral reciprocal lattice. While the basal plane components of these modulation wave vectors exhibit trigonal symmetry, their differing components along the $\mathbf{c}^*$ direction necessarily lower the overall symmetry to triclinic. Such a situation is strongly reminiscent of the $1T_{2/3}$ or so-called stripe state of TaS_2 (13). Note that $\mathbf{q}_1 + \mathbf{q}_2 + \mathbf{q}_3 = \mathbf{0}$ and hence only two of these primary modulation wave vectors are strictly independent. In terms of a conventional space group approach, this S1 superlattice has triclinic symmetry and reciprocal lattice basis vectors that can be chosen to be

$$\mathbf{a}'^* = \mathbf{q}_1 = \tfrac{1}{7}(2\mathbf{a}^* + \mathbf{b}^* + \mathbf{c}^*),$$
$$\mathbf{b}'^* = -\mathbf{q}_3 = \tfrac{1}{7}(-\mathbf{a}^* + 3\mathbf{b}^* - 4\mathbf{c}^*), \quad \text{and}$$
$$\mathbf{c}'^* = 3\mathbf{c}^*.$$

The corresponding real space triclinic unit cell is given by

$$\mathbf{a}' = 3\mathbf{a} + \mathbf{b}, \quad \mathbf{b}' = -\mathbf{a} + 2\mathbf{b}, \quad \text{and} \quad \mathbf{c}' = \tfrac{1}{3}(-\mathbf{a} + \mathbf{b} + \mathbf{c}),$$

where $a' = b' = 10.49$ (10.52), $c' = 9.55$ (9.46) Å, $\alpha' \sim 76.5°$, $\beta' \sim 99.0°$, and $\gamma' \sim 120.0°$ for the M = Ca (Sr) systems using the cell parameters of Table 1 and assuming

that the underlying rhombohedral cell parameters stay metrically rhombohedral.

To within the accuracy of measurement for our TEM (estimated to be ~0.5–1.0%), the underlying subcell stays metrically rhombohedral, i.e., $|(1\bar{2}10)^*| = |(\bar{2}110)^*| = |(11\bar{2}0)^*|$ (note that $|(1\bar{2}10)^*|$ represents the magnitude of the reciprocal lattice vector $(1\bar{2}10)^*$). The broadening of the rhombohedral lines that is invariably observed in such systems regardless of annealing time (9), however, suggests that the triclinic superlattice does give rise to some slight metrical distortion of the underlying rhombohedral subcell. The lack of splitting in the Guinier patterns, however, rules out exact determination of the triclinic cell parameters of this S1 superlattice.

Figure 3 shows the central portion (the ZOLZ region) of an [001] zone axis SADP corresponding to the second S2 type of superstructure. While the basal plane components of the modulation wave vectors have not altered, the intensity distribution of the weak satellite reflections is clearly different from that of Fig. 1a, indicating that the $\mathbf{c}^*$ components of the modulation wave vectors have altered. This is confirmed by detailed tilting experiments and, in particular, by the $[\bar{1}1\bar{2}]$ zone axis SADP and corresponding CBP shown in Fig. 4. The well-defined ZOLZ region and FOLZ ring of Fig. 4b confirm that the primary modulation wave vectors, $\mathbf{q}_j$, characteristic of this superstructure are exactly excited in the ZOLZ region at this particular zone axis orientation (obtained from the [001] orientation of Fig. 3 by a tilt of ~6.95° about the $(11\bar{2}0)^*$ direction of reciprocal space). The FOLZ ring radii in Fig. 4b corresponds to a height along the zone axis direction of $3/|[\bar{1}1\bar{2}]|$ (again as would be expected for the rhombohedral substructure reflections).

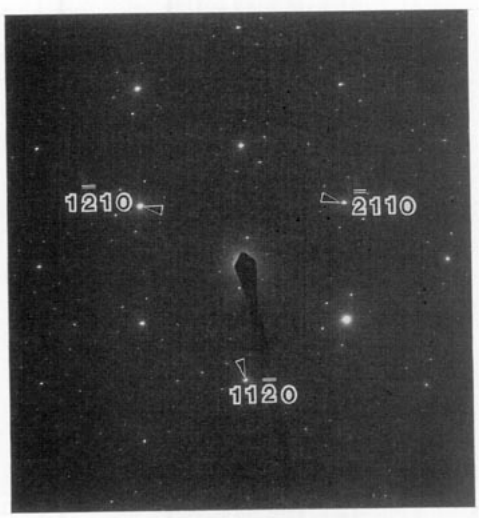

FIG. 3. The central portion (the ZOLZ region) of an [001] zone axis SADP corresponding to the second S2 type of superstructure. The strong reflections corresponding to the rhombohedral parent structure are indexed.

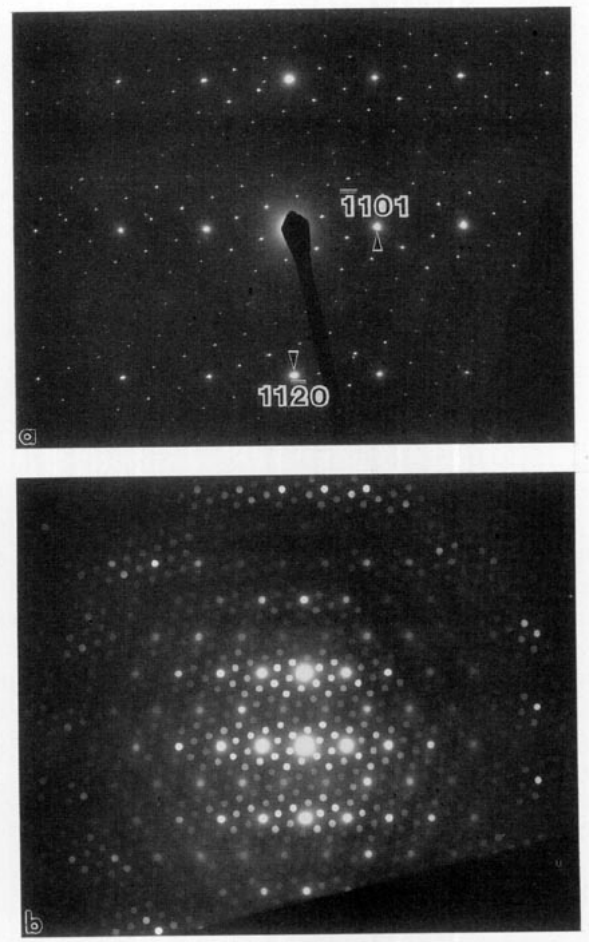

FIG. 4. (a) The central portion (the ZOLZ region) of a $[\bar{1}1\bar{2}]$ zone axis SADP and (b) corresponding CBP for the second S2 type of superstructure. The strong reflections corresponding to the rhombohedral parent structure are indexed in (a).

The reciprocal lattice of this S2 phase can again be described in modulated structure language, i.e., in terms of a strong set of rhombohedral parent reflections $\mathbf{G}$, accompanied by a much weaker set of satellite reflections at $\mathbf{G} \pm \sum m_j\mathbf{q}_j$, where the m_j are integers and where the primary modulation wave vectors $\mathbf{q}_j$ (see Fig. 4a) characteristic of the superstructure are this time given by

$$\mathbf{q}_1 = \tfrac{1}{14}[3(11\bar{2}0)^* - (\bar{1}101)^*] = \tfrac{1}{14}(4\mathbf{a}^* + 2\mathbf{b}^* - \mathbf{c}^*)$$

$$\mathbf{q}_2 = \tfrac{1}{14}[-1(11\bar{2}0)^* + 5(\bar{1}101)^*] = \tfrac{1}{14}(-6\mathbf{a}^* + 4\mathbf{b}^* + 5\mathbf{c}^*)$$

and

$$\mathbf{q}_3 = \tfrac{1}{14}[-2(11\bar{2}0)^* - 4(\bar{1}101)^*] = \tfrac{1}{14}(2\mathbf{a}^* - 6\mathbf{b}^* - 4\mathbf{c}^*).$$

While the basal plane components of these modulation wave vectors are as before, the differing components along the $\mathbf{c}^*$ direction again lowers the overall symmetry to triclinic. Again note that $\mathbf{q}_1 + \mathbf{q}_2 + \mathbf{q}_3 = \mathbf{0}$ and hence

only two of these primary modulation wave vectors are independent. In terms of a conventional space group approach, the reciprocal lattice basis vectors of this S2 superlattice can be chosen to be

$$\mathbf{a}''^* = \mathbf{q}_1 = \tfrac{1}{14}(4\mathbf{a}^* + 2\mathbf{b}^* - \mathbf{c}^*),$$
$$\mathbf{b}''^* = -\mathbf{q}_3 = \tfrac{1}{14}(-2\mathbf{a}^* + 6\mathbf{b}^* + 4\mathbf{c}^*), \quad \text{and}$$
$$\mathbf{c}''^* = \tfrac{3}{2}\mathbf{c}^*.$$

The corresponding real space triclinic unit cell is given by

$$\mathbf{a}'' = 3\mathbf{a} + \mathbf{b}, \ \mathbf{b}'' = -\mathbf{a} + 2\mathbf{b}, \quad \text{and} \quad \mathbf{c}'' = \tfrac{1}{3}(\mathbf{a} - \mathbf{b} + 2\mathbf{c}),$$

where $\mathbf{a}'' = \mathbf{b}'' = 10.42$ (10.50), $\mathbf{c}'' = 18.71$ (19.01) Å, $\alpha'' \sim 96.8°$, $\beta'' \sim 85.5°$, and $\gamma'' \sim 120.0°$ for the M = Ca (Sr) systems, using the cell parameters of Table 1 and again assuming that the underlying rhombohedral cell parameters stay metrically rhombohedral. Again, to within the accuracy of measurement for our TEM, the underlying subcell stays metrically rhombohedral, i.e., $|(1\bar{2}10)^*| = |(\bar{2}110)^*| = |(11\bar{2}0)^*|$. The broadening of the rhombohedral lines in Guinier patterns, however, again suggests that the triclinic superlattice does give rise to some slight metrical distortion of the underlying rhombohedral subcell.

Note that the $C2/m$, $a = 13.653$, $b = 7.866$, $c = 9.554$ Å, and $\beta = 103.76°$ supercell reported for $Ca_{0.176}Bi_{0.824}O_{1.412}$ by Blower and Greaves (12) corresponds to

$$\mathbf{a}' = 2\mathbf{a} - 2\mathbf{b}, \quad \mathbf{b}' = 2\mathbf{a} + 2\mathbf{b}, \quad \text{and} \quad \mathbf{c}' = \tfrac{1}{3}(-\mathbf{a} + \mathbf{b} + \mathbf{c})$$

and is not compatible with either the S1 or S2 variety of superstructure.

Figure 5 shows (a) [001], (b) $\langle 1\bar{1}2\rangle$, (c) an $\sim\langle\bar{4}49\rangle$, and (d) $\langle\bar{1}11\rangle$ zone axis CBPs typical of the third, rather more complicated, S3 variety of modulated structure, found for the $x = 0.250$ specimen in the M = Sr system. Individual grains of this specimen were found to be rather buckled by comparison with grains of the S1 and S2 specimens. To minimize orientational averaging while at the same time maintaining reasonable resolution in reciprocal space, CBPs were taken using a small condenser aperture. Detailed tilting experiments show that the resultant structure maintains the rhombohedral symmetry of the parent

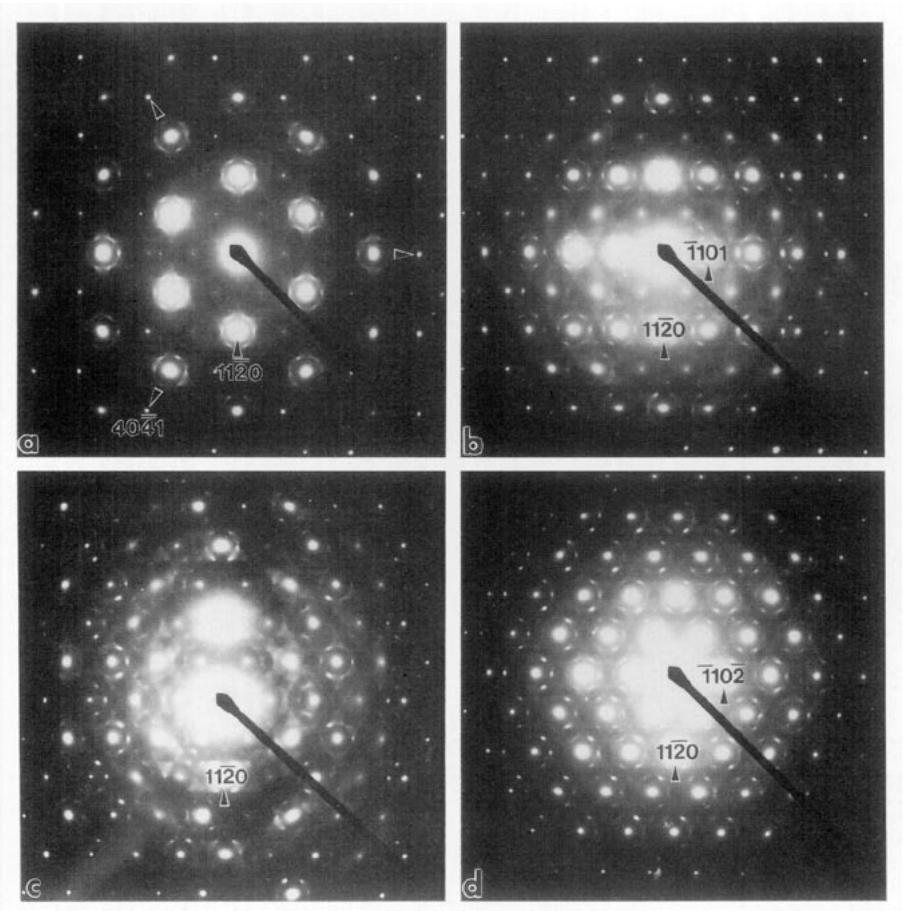

FIG. 5. (a) [001], (b) $\langle 1\bar{1}2\rangle$, (c) $\sim\langle\bar{4}49\rangle$, and (d) $\langle\bar{1}11\rangle$ zone axis CBPs typical of the S3 type of superstructure. Strong reflections corresponding to the rhombohedral parent structure are indexed.

structure, i.e., tilting about any one of the three possible $\{11\bar{2}0\}^*$ systematic rows of Fig. 5a always gives rise to the same sequence of CBPs, for the same tilt angle, as shown in Figs. 5b–5d. Unlike the case for the S1 and S2 superstructures, however, the additional satellite reflections are by no means sharp but always somewhat smeared out. In addition, they are always accompanied by a rather spectacular diffuse intensity distribution (see, for example, Figs. 5c and 6). Indeed the apparent superlattice reflections are clearly not independent of the diffuse distribution but rather represent maxima in it.

The basal plane components of the apparent primary modulation wave vectors of this S3 phase (see Fig. 5a) are now incommensurate with respect to the reciprocal lattice of the underlying parent structure and are given, to an accuracy of ~1%, by

$$\mathbf{q}_{1b} \sim 0.350\ \mathbf{a}^*, \quad \mathbf{q}_{2b} \sim 0.350\ (-\mathbf{b}^*), \quad \text{and} \quad \mathbf{q}_{3b} \sim 0.350\ (-\mathbf{a}^* + \mathbf{b}^*).$$

Baggio *et al.* (11) similarly report incommensurate primary modulation wave vector basal plane components for the M = Sr system, but only for $x > \sim 0.33$ (see Fig. 2 of (11)). The above primary modulation wave vector basal plane components correspond to those reported by Baggio *et al.* (11) for $x \sim 0.40$! The reason for this discrepancy is unclear.

The extent of ordering along the $\mathbf{c}^*$ direction, however, is very difficult to determine given the buckled nature of the specimens and the fact that only zone axis orientations relatively close to [001] are obtainable. The three apparently strongly excited satellite reflections labeled 1, 2, and 3 in the $\langle 5\bar{5}4\rangle$ zone axis CBP shown in Fig. 6, for example, index as $(2\bar{1}\bar{1}3)^* + \mathbf{q}_3$, $(2\bar{1}\bar{1}3)^* - \mathbf{q}_1$, and $(2\bar{2}0\bar{5})^* + \mathbf{q}_2$ respectively. Assuming that these satellite reflections belong to the ZOLZ at this zone axis orientation, the corresponding modulation wave vector components along $\mathbf{c}^*$ would be $q_{1z} \sim 0.31$, $q_{2z} \sim -0.44$, and $q_{3z} \sim 0.12$. On the other hand, the satellite reflections excited at the $\langle 1\bar{1}2\rangle$ zone axis orientation of Fig. 5b imply q_z components of ~ -0.18 and 0.35, respectively, while the satellite reflections excited at the $\langle\bar{1}11\rangle$ zone axis orientation of Fig. 5d imply q_z components of ~0.35 and −0.70, respectively. Such an array of required q_z components suggests a more or less continuous (along $\mathbf{c}^*$) rod of intensity centered on the $\mathbf{G} \pm \mathbf{q}_{jb}$ positions of reciprocal space with maxima in intensity around at least the q_z values given above. Given the existence of the accompanying diffuse distribution as well, it is clear that there is a considerable amount of disorder associated with this phase in contrast with the extremely well-ordered S1 and S2 phases. Further consideration of this phase, however, is beyond the scope of the current paper.

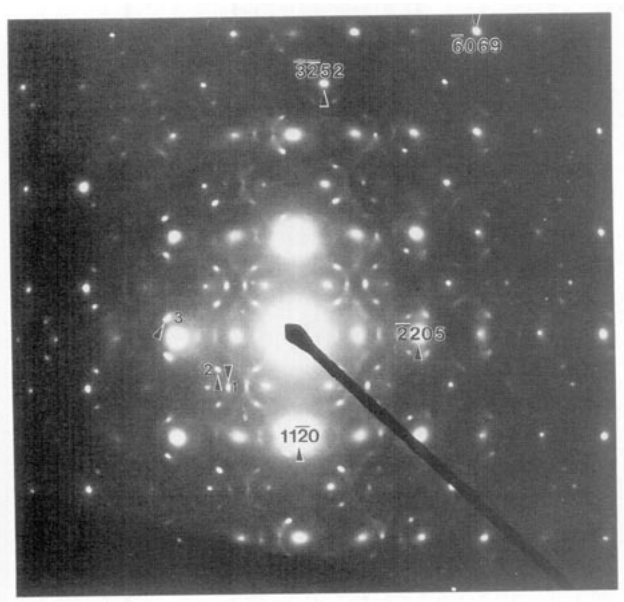

FIG. 6. A $\langle 5\bar{5}4\rangle$ zone axis CBP typical of the S3 type of superstructure. Strong reflections corresponding to the rhombohedral parent structure are indexed.

4. REAL SPACE INTERPRETATION

While the average metal atom array of such systems is well defined (2, 7, 8), there is still considerable uncertainty as to the average oxygen atom array. Apart from the early work of Aurivillius and colleagues (1, 2), there has been only one average structure refinement of a composition within the β type solid solution for either the Bi_2O_3–SrO or Bi_2O_3–CaO systems. This X-ray refinement was of $Bi_{0.765}Sr_{0.235}O_{1.383}$ (7). Rhombohedral $R\bar{3}m$ space group symmetry (with $a \sim 4$ Å and $c \sim 28$ Å in the hexagonal setting) was used. Two crystallographically distinct, fully occupied, metal atom sites (M1 and M2) were found. (The stacking of these fully occupied metal atom layers along the c axis ia (ABC)(BCA)(CAB) giving the nine-layer, ~28 Å repeat.) Only Bi is found to occupy the M2 site whereas mixed Bi/M (M = Sr or Ca) metal atom occupancy is found for the M1 site (see Fig. 7). Given that this refinement used X-rays (7), it is not surprising that it was much more difficult to locate oxygen atom positions. Two oxygen atom sites (O1 and O2) were found (see Fig.7).

If both these sites were fully occupied, the average structure could be described as being built up of three-metal-atom-layer thick M_3O_4 slabs of fluorite type which are themselves stacked in an ABC manner (7, 8). Site O2, however, was found to be partially occupied with an estimated occupancy of ~$\frac{1}{3}$. As the authors themselves point out, only ~$\frac{2}{3}$ of the oxygens that must be present were therefore found. It was suggested that the remaining oxygens must be located either near octahedral sites

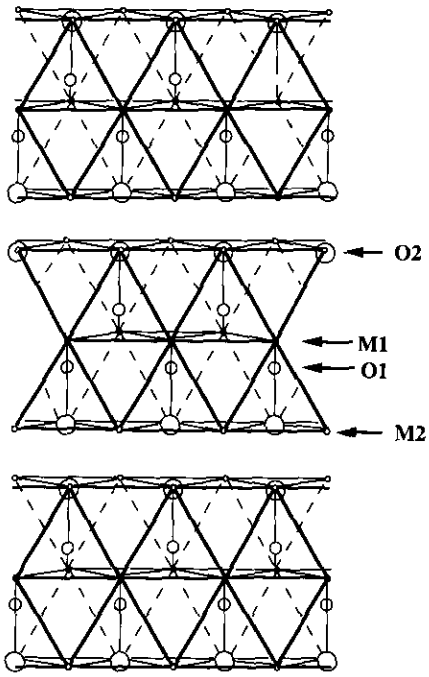

FIG. 7. A view (approximately down ⟨110⟩) of the average rhombohedral structure. The $(-\mathbf{b} + \mathbf{c})$ direction is horizontal and the $\mathbf{c}$ direction is vertical. Small circles are metal atom sites, medium circles are O1 sites, and large circles are O2 sites. The crystallographically distinct M1, M2, O1, and O2 sites are labeled.

within the M_3O_4 slabs or near tetrahedral or octahedral sites between these slabs. Sites of such type were indeed found to be partially occupied in the neutron powder refinements of $Ca_{0.176}Bi_{0.824}O_{1.412}$ (12) and the closely related $Bi_{0.7}La_{0.3}O_{1.5}$ (8). (Note that the monoclinic supercell used for the refinement of $Ca_{0.176}Bi_{0.824}O_{1.412}$ (12) is not compatible with either of the S1 or S2 superstructures described above. Features of this refinement associated with the average rhombohedral structure, in particular the oxygen occupancy of sites other than O1 or O2, should nonetheless still be reliable.)

Given this lack of knowledge as to the average occupancies and positions of all the oxygen atom sites, it is not yet possible to present a coherent story as regards the real space origin of the observed superstructures. The most obvious possible source of the additional superstructure reflections is Bi/M ordering within the mixed metal atom layers (9). Such compositional modulation, however, is almost certainly accompanied by oxygen vacancy ordering as well as associated structural relaxation. That considerable structural relaxation must be associated with Bi/M ordering can be deduced from the apparent valences (AVs; see (14)) of the (6 + 2) coordinated M1 site depending upon whether the site is occupied by Bi or Sr. For Bi occupancy, the refined average structure (7) gives an AV of 2.06 whereas, for Sr occupancy, the corresponding AV is 2.22. Clearly, Bi is heavily underbonded, whereas Sr is somewhat overbonded in the M1 site. In either case, substantial relaxation of the surrounding oxygen atom array needs to take place to satisfy local bonding requirements.

Formally the deviation of the resultant structure from the average structure must be expressed in terms of compositional and displacive modulations as (15)

$$\delta f_\mu(\mathbf{T}) = f_\mu^{\text{av}} \text{Re}\left\{\sum_q a_\mu(\mathbf{q}) \cos(2\pi\mathbf{q}\cdot\mathbf{T} + \theta_\mu(\mathbf{q}))\right\} \quad [1]$$

$$\mathbf{u}_\mu(\mathbf{T}) = \text{Re}\left\{\sum_q \sum_{\alpha=a,b,c} \boldsymbol{\alpha}\varepsilon_{\mu\alpha}(\mathbf{q}) \cos(2\pi\mathbf{q}\cdot\mathbf{T} + \theta_{\mu\alpha}(\mathbf{q}))\right\} \quad [2]$$

where $\delta f_\mu(\mathbf{T})$ represents the deviation (from f_μ^{av}) of the atomic scattering factor of the μth atom in the $\mathbf{T}$th parent primitive unit cell, while $\mathbf{u}_\mu(\mathbf{T})$ represents the atomic displacement away from its position in the parent structure $(\mathbf{r}_\mu + \mathbf{T})$ of the μth atom in the $\mathbf{T}$th parent primitive unit cell. If such modulations have nonzero amplitude, they will give rise to satellite reflections at $\mathbf{G} \pm \mathbf{q}$, where $\mathbf{G}$ is a *Bravais-lattice-allowed* reflection of the average rhombohedral structure.

In order to give some tentative indication of the possible real space origin of the additional satellite reflections, Bi/M ordering within the mixed metal atom layers is focused upon in what follows. Consider a general composition $Bi_{1-x}M_xO_{1.5-0.5x}$, where M = Sr, Ca, or Ba. Two out of every three metal atom layers perpendicular to $\mathbf{c}$ are pure Bi. Therefore the average atomic scattering factor of a metal atom in the mixed metal atom layers $f^{\text{av}} = 3xf_M + (1 - 3x)f_{\text{Bi}}$. The resultant occupancies can then formally be expressed in terms of Eq. [1].

In the case of the S1 type superstructure, the only three modulation wave vectors that need to be considered are $\mathbf{q}_1$, $\mathbf{q}_2$, and $\mathbf{q}_3$ as given in Section 3 above. Substituting $\mathbf{T} = x\mathbf{a} + y\mathbf{b} + z\mathbf{c}$ (hexagonal notation) give

$$\begin{aligned} f = f^{\text{av}}\{1 &+ a_1 \cos(2\pi/7[2x + y + z] + \theta_1) \\ &+ a_2 \cos(2\pi/7[-3x + 2y - 5z] + \theta_2) \\ &+ a_3 \cos(2\pi/7[x - 3y + 4z] + \theta_3)\} \end{aligned}$$

If three-fold symmetry of the Bi/M ordering pattern within any one mixed metal layer perpendicular to $\mathbf{c}$, e.g, $z = 0$, is assumed (not necessarily the case) then $a_1 = a_2 = a_3 = a$ and $\theta_1 = \theta_2 = \theta_3 = \theta$. Choosing $\theta = -69.296°$, $x = \frac{1}{7} = 0.143$ and $f^{\text{av}}\ a = -\frac{4}{7}(f_{\text{Bi}} - f_M)$, for example, gives rise to the Bi/M ordering pattern shown in Fig. 8, i.e., clustering of M atoms into triangular clusters. (It may be that the apparent stability of the $\sqrt{7} \times \sqrt{7}$ basal plane supercell common to both the S1 and S2 type of superstructures is tied up with the common occurrence of such triangular clusters of M atoms.) The three-dimensional

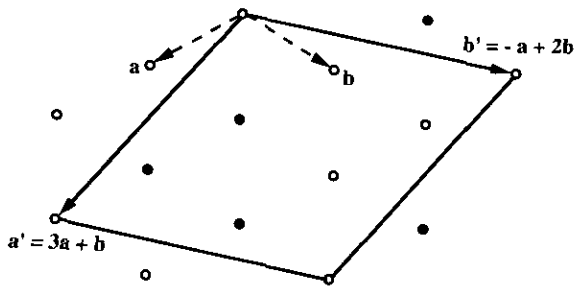

FIG. 8. Schematic illustration of the Bi/*M* ordering pattern resulting from the choice of modulation wave amplitudes and phases described in the text. The empty circles represent Bi atoms and the filled circles represent *M* atoms. The mixed metal layer shown is projected normal to the hexagonal **c** axis. The hexagonal basal plane supercell is shown as well as the basal plane unit cell vectors of the average structure.

distribution is then obtained by stacking this Bi/*M* distribution according to the $\mathbf{c}' = \frac{1}{3}(-\mathbf{a} + \mathbf{b} + \mathbf{c})$ S1 supercell vector. Whether such a Bi/*M* distribution does or does not actually occur, however, can only be determined by a full supercell structure refinement.

Note that a fully ordered Bi/*M* distribution of this type only occurs for $x = \frac{1}{7}$ exactly. Any other value of x, e.g., $x = 0.13$ as for the *M* = Ca specimen, necessarily entails partial occupancies. The exact solid solution width in x of the S1 and S2 type superstructures has not been determined in this paper. The observation of only S1 and S2 superstructures in the current work despite the investigation of a range of values of x, however, suggests that both the S1 and S2 superstructures each exist over a significant range of x.

In the case of the S2 superstructure, the basal plane supercell is the same as for S1 (see Fig. 8). The stacking vector, however, is now $\frac{1}{3}(\mathbf{a} - \mathbf{b} + 2\mathbf{c})$ rather than the $\frac{1}{3}(-\mathbf{a} + \mathbf{b} + \mathbf{c})$ stacking vector of S1. Hence there are now two distinct mixed metal atom layers which need not have the same occupancy of *M* atoms. Given that the S2 type of superstructure occurs for larger values of x, it is clear that the average *M* occupancy of the mixed metal atom layers must be increasing. There are numerous ways in which this could happen, e.g., one could envision a structure with one mixed metal atom layer as above, i.e., clustering of *M* atoms into triangular clusters and an *M* occupancy of $\sim\frac{3}{7}$, followed by another layer with an increased *M* occupancy of, say, $\frac{6}{7}$, i.e., all atoms *M* except for the atoms at the corner of the supercell (see Fig. 8). Such a Bi/*M* ordering pattern would correspond to an x of $\frac{3}{14}$ or 0.214. If one tries to avoid partial occupancies, there would probably need to be a whole series of "quantized" superstructures rather than a solid solution. Experimentally, however, there is no evidence for such a series of superstructures, e.g., both S1 and S2 superstructures can clearly exist at different values of x. Similarly, the systems show an apparently continuous variation of average structure lattice parameters as a function of composition (*1*). Further understanding of these fully ordered S1 and S2 superstructures, however, must await the results of full supercell structure refinements.

The disordered nature of the S3 type of superstructure makes it even more difficult to speculate about. The magnitude of the basal plane modulation wave vector, i.e., $0.350a^*$, is presumably related to the average basal plane separation distance ($1/0.350a^* = 2.47a < \sqrt{7}a = 2.646a$) of clusters of *M* atoms. Long-range order, however, is clearly lost. In this case, it is difficult to see how further progress can be made without quantitative measurement and modeling of the diffuse distribution.

REFERENCES

1. L. G. Sillen and B. Aurivillius, *Z. Kristallogr.* **101,** 483 (1939).
2. B. Aurivillius, *Ark. Kemi. Mineral. Geol. A* **16,** 1 (1943).
3. E. M. Levin and R. S. Roth, *J. Res. Nat. Bur Stand Sect. A* **68,** 197 (1964).
4. T. Takahashi, H. Iwahara, and Y. Nagai, *J. Appl. Electrochem.* **2,** 97 (1972).
5. P. Conflant, J-C. Boivin, and D. Thomas, *J. Solid State Chem.* **18,** 133 (1976).
6. R. Guillermo, P. Conflant, J-C. Boivin, and D. Thomas, *Rev. Chim. Miner.* **15,** 153 (1978).
7. P. Conflant, J-C. Boivin, and D. Thomas, *J. Solid State Chem.* **35,** 192 (1980).
8. D. Mercurio, M. El Farissi, J. C. Champarnaud-Mesjard, B. Frit, P. Conflant, and G. Roult, *J. Solid State Chem.* **80,** 133 (1989).
9. R. J. D. Tilley, *J. Solid State Chem.* **41,** 233 (1982).
10. P. Conflant, J-C. Boivin, G. Nowogrocki, and D. Thomas, Proceedings, 6th Risoe International Symposium on Metallurgy and Materials Science, 1985, p.285.
11. R. Baggio, G. Leyva, and F. Parisi *in* "Methods of Structural Analysis of Modulated Structures and Quasicrystals" (J. M. Pérez-Mato, F. J. Zúñiga, and G. Madariaga, Eds.), p. 433. World Scientific, Singapore, 1991.
12. S. K. Blower and C. Greaves, *Mater. Res. Bull.* **23,** 765 (1988).
13. R. L. Withers and J. W. Steeds, *J. Phys. C* **20,** 4019 (1987).
14. N. E. Brese and M. O'Keeffe, *Acta Crystallogr. Sect. B* **47,** 192 (1991).
15. J. M. Pérez-Mato, G. Madariaga, F. J. Zúñiga and A. Garcia Arribas, *Acta Crystallogr. Sect. A* **43,** 216 (1987).